Self-Powered Electronic Skin with Biotactile Selectivity

*Kesong Hu, Rui Xiong, Hengyu Guo, Ruilong Ma, Shuaidi Zhang, Zhong Lin Wang, and Vladimir V. Tsukruk**

Tactile sensing materials are critically important for human–machine interfacing components of wearable and portable electronics, smart automation servers, soft robotics, and active identifications.[1–3] Generally, piezoelectricity,[4–7] piezoresistivity,[8–10] capacitance,[11,12] chemomechanics,[13,14] and triboelectrification[15–17] are the major fundamental mechanisms exploited for tactile/approximate sensing ability, which show different characteristics in specialized applications.[18] However, most of these sensors not only rely on external power supply but also require signal processing/amplification additions due to the minute signal amplitude generated by the underlying sensing mechanisms.[19] Self-powered (or "zero-power") sensing and enhanced responses are required for constructing sustainable nodes for the fast growing internet-of-things, such as wearable body monitors, intelligent home appliances, smart logistic tags, and active surveillance networks.[20–22] Although numerous tactile sensors detect various local pressure events, the difficulty for the differentiation between human and artificial touches remained a major challenge due to the lack of selective response for unique biological interfacial cues.[23,24] Humidity and temperature sensors can be adopted as human tactile sensors due to the distinctive moisture and temperature on the human body surface, but the response rate of the humidity or temperature sensors is usually modest due to the relatively slow water adsorption/desorption or thermal dissipation processes.[25–27] The search for functional materials suitable for biointerfacial sensing which facilitate self-powered autonomous devices for human-technology interfaces has not been completed yet.

One of the recent candidates for the role of active materials compatible with biointerfaces is graphene and its derivatives which are non-biotoxic and flexible. These robust and flexible materials have been playing an important role in various structural and functional applications due to their extraordinary electrical, mechanical, and chemical properties.[28–30] Sensors,[31] batteries,[32,33] supercapacitors,[34] and multifunctional nanocomposites[35] fabricated using graphene-based materials hold promises for a wide range of applications. For instance, flexible strain sensors made using graphene as the active component have been reported extensively.[31] However, pristine graphene based functional structures usually require tedious assembly and packaging processes.[36] As an alternative material from the graphene class, graphene oxide (GO) is primarily used as a precursor for reduced graphene oxide (rGO) to fabricate mechanically robust and electrically conductive nanocomposites.[37–39] Recently, flexible bioenabled graphene oxide paper with outstanding mechanical properties and high electrical conductivity has been introduced.[40,41] The electrically conductive patterns can be formed by the metal-assisted spontaneous electrochemical reaction technique.[41] Owing to the galvanic nature of the metal–GO reactions, the activation of the power generation under wet conditions can be utilized for self-powered humidity and biotactile sensing materials.

Herein, we introduce novel self-powered tactile sensing materials based on the ultrathin metal–GO junctions that serve as the microreactors for the localized electrolyte-triggered electrochemical reactions. These sensing materials exclusively respond to direct touching of human fingers, which delivers trace amount of bioelectrolytes to trigger the metal–GO electrochemical reactions. A supplementary voltage output by the spontaneous diffusion of protons widens the available electrode materials to noble metal (Au) and semi-metallic rGO components. The metal–GO junctions show stable high-level response (up to 1000 mV) for both static and dynamic (up to 20 Hz frequency) tactile events. These ultrathin graphene-based materials show the excellent mechanical robustness, flexibility, and foldability, which make them suitable for autonomous electronic skins in soft robotics structures that do not need external power supply in standby and operation modes.

GO biopaper has been fabricated by vacuum filtration of the GO aqueous suspension with 2.5 wt% of silk fibroin (SF) as biobinders. The strong binding interactions, high mechanical properties, and inherent chemical inertness of the SF are excellent to strengthen GO paper while minimizing the affection to its chemical properties.[40] The tactile sensing hybrid materials have been assembled by depositing two separate thin metal electrodes on the surface of the laminated GO biopaper (**Figure 1**a), forming a metal–GO junction pair with various gap widths.

The uniform 500 nm thick metal layers of different nature were deposited by electron-beam evaporation on the GO biopaper (Figure 1b; Figure S1 and S2, Supporting Information). The excellent flexibility of the metal–GO junctions facilitates

Dr. K. Hu, R. Xiong, H. Guo, R. Ma, S. Zhang, Prof. Z. L. Wang, Prof. V. V. Tsukruk
School of Materials Science and Engineering
Georgia Institute of Technology
Atlanta, GA 30332-0245, USA
E-mail: vladimir@mse.gatech.edu

R. Xiong
State Key Laboratory of Polymer Materials Engineering
Polymer Research Institute of Sichuan University
Chengdu 610065, P. R. China

H. Guo
Department of Optoelectronic Engineering
Chongqing University
Chongqing 400044, P. R. China

Prof. Z. L. Wang
Beijing Institute of Nanoenergy and Nanosystems
Chinese Academy of Sciences
Beijing 100083, P. R. China

DOI: 10.1002/adma.201506187

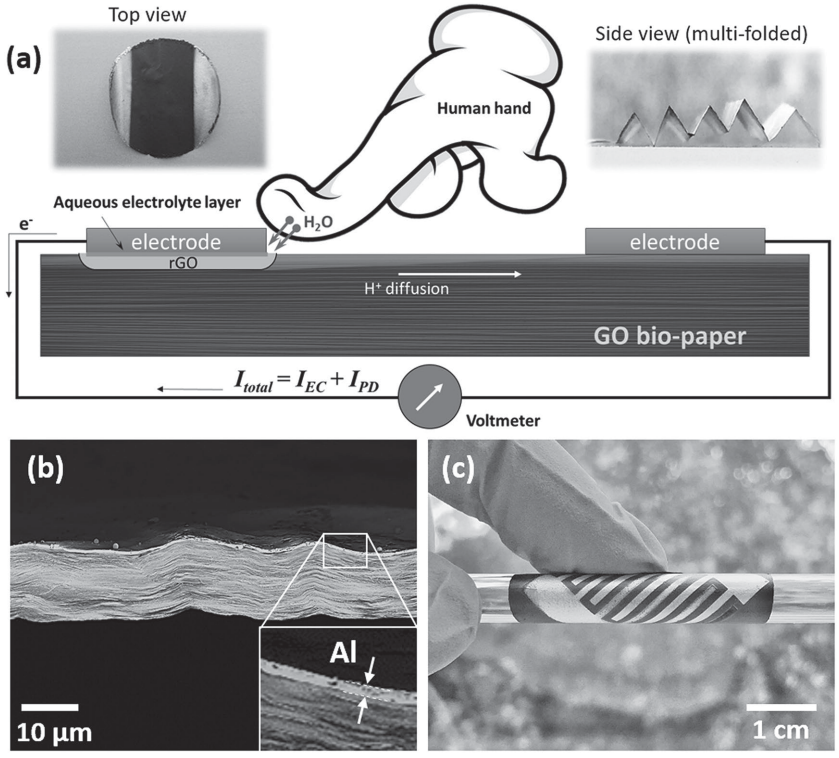

Figure 1. a) The metal–GO junction structure and the mechanism of power generation. Insets: (left) the top view of the symmetrical Al–GO junction pair, and (right) the side view of the same sample that shows its excellent folding robustness. b) SEM micrograph showing the cross-section of an Al–GO junction. The inset emphasizes the uniform Al coating layer. c) Optical photograph demonstrating the flexibility of the Au/Al-coated GO biopaper.

conformity to curved surfaces that does not affect sensing performance (Figure 1c) (see below). Moreover, complete folding–unfolding do not compromise the integrity of the films (Figure 1a inset; Figure S3, Supporting Information). When the metal–GO junctions are moisturized by either directly tapping deionized water (macroscopic moisturizing) or pressing with a bare finger (microscopic moisturizing) (Figure 1a), an electrical potential (the "voltage output") of few hundred millivolts can be detected with polarity depending upon touch location (right or left junction).

The analysis of the output combinations allows us to explore the mechanism of the tactile sensing behavior (**Figure 2**). As observed in Figure 2a, upon finger pressings, all three symmetrical junction pairs made with various metals show stable output signal levels throughout the prolonged activation period (60 s) for opposite junctions. For the three metal electrode materials we have tested, gold (Au), copper (Cu), and aluminum (Al) generate sequentially larger potential outputs (Figure 2a). The overall activation rate of the Al–GO junction is 605 mV s^{-1}, and the deactivation rate of the same junction is around 400 mV s^{-1}, conforming fast recovery that is critical for repeated activations (see below). What is also important is that the output of the opposite metal–GO junctions has the same amplitude but opposite polarity compared to that of the positive electrode, demonstrating the universal response of the metal–GO junctions without the need of electrode calibration.

It is also worth noting that replacing a human finger with finger shaped sponge wetted by water or salt solutions results in the increase of voltage output depending on the concentration of the salt in the solution (Figure S4, Supporting Information). Higher sodium chloride (NaCl) concentration results in higher voltage output. The 800 mV signal level caused by bare finger matches that of the 0.25–0.5 wt% NaCl solution, which is the estimated salt concentration of human perspiration (bioelectrolyte).[42] These changes indicate that water is the key component for the activation event and the addition of the bioelectrolyte from the human skin enhances it. Figure 2b shows that by narrowing the gap between the Al–GO junctions from 24 to 6 mm, the voltage output increases to a very high value of about 1000 mV that makes signal detection very robust and easy. As mentioned earlier, the addition of silk fibroin to the GO paper is solely for mechanical reinforcement under moist conditions, the electrical signals are not affected by silk fibroin as demonstrated in Figure S5 (Supporting Information).

Considering the large difference between the outputs when the aluminum and gold metals are in use (610 mV difference according to Figure 2a), asymmetrical Au/Al–GO junction pair has further been fabricated as a simple ambient humidity sensor (Figure 1c and 2c, inset). The interdigitated finger pattern for the metal layers has been designed to maximize the perimeter of the junctions, where the water vapor gets transported to the metal–GO interface to initiate the electrical response. For this design, we observed that the relative humidity increases from near 0 to about 100 RH% by 1 RH% min^{-1} resulted in step-like increase in the output voltage from 0 to 160 mV within a narrow relative humidity window from 35% to 45%, indicating an abrupt process of the formation of continuous surface water layer (Figure 2c). The ambient humidity and the response also showed some hysteresis related to slower surface water layer desorption during drying.[47]

Based on the phenomena demonstrated in Figure 2a–c and results from our previous study,[41] we propose the primary working mechanism be the electrochemical reaction between the active metal electrodes (Al and Cu) and the GO surface as has been suggested for different materials combinations.[40,41] Indeed, for such an interface, a direct touch event with a bare finger results in delivery of trace amount of bioelectrolytes (primarily from perspiration) to the GO surface at the electrode junction (Figure 1a). The solubilized GO surface ionizes to form an ultrathin electrolyte fluid layer between the reactive metal anode and the GO cathode, generating electrochemical potential that drives current flow through the external circuit. Al–GO junctions show the highest output of over 800 mV due to the largest reduction potential gap between aluminum and GO surface (around 1.0 V).[40] Copper can also reduce GO surface but has much smaller reduction potential gap (0.21 V[43]), thus the output of the Cu–GO junction is moderate (around 300 mV).

Adv. Mater. **2016**,
DOI: 10.1002/adma.201506187

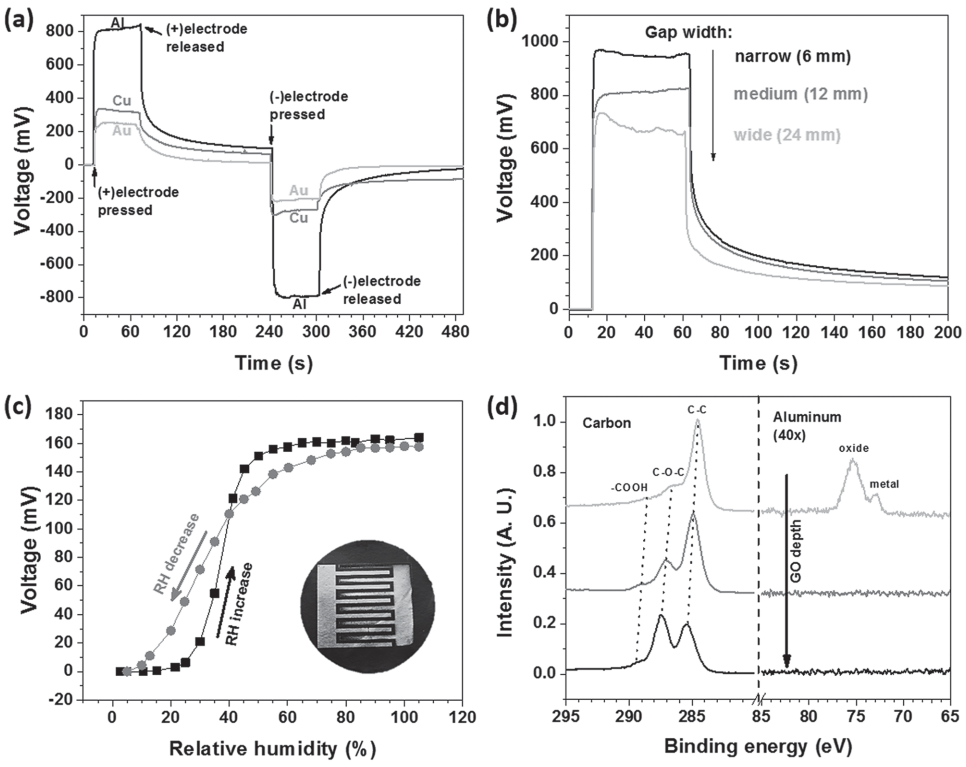

Figure 2. Open-circuit voltage outputs of the metal–GO junction pairs with various (a) electrode metals and (b) gap widths between electrodes. c) The voltage response of an asymmetrical Au/Al–GO junction pair to humidity change (1 RH% min^{-1}), showing slight hysteresis due to the faster water adsorption than desorption (inset: optical photograph of the Ø37mm sample). d) XPS spectra of an extensively actuated (around 5000 times) Al–GO junction at different depths from the Al/GO interface, indicating a reduced layer of GO underneath the Al coating. The blueshift of the carbon peaks indicates the progressive charging effect due to the removal of the electrically conductive layers.

In the case of Au–GO junctions, no electrochemical reaction happens,[43] but the output voltage is still notably high at around 250 mV probably due to the additional ion diffusion.[41] The microinjection of water by bare finger touch dissolves the top few layers of GO in the contacted area, producing GO^{n-} anions and H^+ cations due to the carboxyl groups on GO.[35] We suggest that the gradient of the protons (i.e., dc_{H^+}/dL, where c_{H^+} is the initial concentration of protons upon dissolution and L is the diffusion distance) across the two junctions can cause the diffusion-induced voltage output with the distance between the junctions affecting the electrical voltage output (Figure 2b).[44] The dissociated protons from the ionized carboxyl groups of GO surfaces diffuse from the ionized area around the touched electrode to the opposite electrode driven by the concentration gradient, forming the secondary potential difference between the two electrodes. By narrowing the gap between the Al–GO junctions from 24 to 6 mm, the voltage output increase linearly from 680 to 950 mV, resulting in a 14.4 mV mm^{-1} sensitivity to the gap distances. This correlation between the output amplitude and the junction distance further demonstrates the additional voltage contribution from the proton diffusion. Moreover, the polarity of the proton diffusion current (I_{PD}) matches that of the electrochemically-induced current (I_{EC}), enhancing the signal strength of the touching activation (Figure 1a). Due to the large internal resistance of the GO substrate (over 200 MΩ), the short circuit current (I_{SC}) of the fully activated Al–GO junction is around 55 nA, which is hard to detect using simple portable devices for wearable electronics applications (Figure S6, Supporting Information). On the other hand, the open-circuit voltage (V_{OC}) of the same fully activated Al–GO junction reaches 900 mV that is easily measured and transduced for sensing and actuation purposes. Therefore, we use V_{OC} as the standard output for signal analysis.

In order to monitor the change of the chemical composition after the tactile actuations, the GO surface beneath the aluminum coating has been characterized by the depth-resolved X-ray photoelectron spectroscopy (XPS) (Figure 2d; Figure S7, Supporting Information). XPS showed the extinction of the epoxy peak at around 286.5 eV that indicates full reduction of the topmost regions of GO substrate in contact with the aluminum layer.[45] Deeper layers of GO substrate gradually turn from completely reduced state to partially reduced state, and eventually to fully intact oxidized state. The gradual chemical reduction of the GO layers is the direct evidence of the electrochemical reaction triggered by moisture injection. No such reduction gradient for either the newly assembled Al–GO junction or long-term used Au–GO junction is detected, indicating the exclusive electrochemical reaction happening at the Al–GO interfaces during the tactile actuations (Figure S8, Supporting Information).

The overall operation mechanism of the metal–GO junction pairs for tactile sensing can be summarized by equivalent circuit diagrams (Figure S9, Supporting Information). When idle in dry air, no electrochemical reaction or proton diffusion

happen due to the lack of water; thus, no voltage output could be detected (Figure S9a, Supporting Information). When the air is moist (>45 RH%), the adsorption of water from the air on the metal–GO junction starts to trigger the electrochemical reactions only for the reactive metals (e.g., Al and Cu). Due to the opposite polarity of the two identical "galvanic cells", the measured voltage output is still minimal, demonstrating great "auto-zero" characteristic regardless of the environment humidity (Figure S9b, Supporting Information). However, if the two metal electrodes are not the same, the asymmetrical junction pairs will output voltage signal as shown in Figure 2c. In the case of single junction actuation by bare finger press, stronger electrochemical reaction is triggered due to the sudden flux of bioelectrolyte injection and the protons start to diffuse to the opposite electrode, generating strong synergistic electrical potential that could be detected by voltmeter with differentiation of the activated junction (positive or negative voltage readings) (Figure S9c, Supporting Information). If the electrode is inert to GO, like Au and rGO, only the potential generated by the proton diffusion happens, which is much smaller without the electrochemical reaction. Lastly, when the two junction are pressed simultaneously, no voltage output is detected due to the total cancelling of the symmetrical opposite potentials (Figure S9d, Supporting Information).

It is important to note that the GO humidity sensors reported to date are based on very different foundations and usually request additional signal processing and amplification. For instance, an impedance type polyelectrolyte/graphene bilayer sensors measured ultralow humidity with linear signal output.[46] Zhao et al. recently reported an active humidity sensor using gradient rGO film, which records human breath humidity as induced by the diffusion of dissociated protons.[44] However, the signal amplitude is an order of magnitude lower than the Al–GO junction demonstrated here, probably due to the extremely large internal impedance of these systems. Another ultrafast humidity sensor has been fabricated by depositing ultrathin GO films on printed silver electrodes.[47] Due to the fast water adsorption and desorption on the ultrathin GO surface, the impedance changes with the relative humidity with moderate sensitivity reported. The power-generating humidity sensing mechanism observed here is based on sensitive electrolyte-triggered electrochemical reactions at the metal–GO interface, setting apart this materials design.

The symmetrical Al–GO junction and the asymmetrical Au/Al–GO junction electrode pairs were further characterized under two repeated actuation patterns of switching and alternating (**Figure 3**).

For the switching tests, the positive junction was repeatedly pressed by the bare finger 30 times and then the repeated presses were switched to the negative junction for another 30 times with the 1 s dwell and interval times. The stable voltage output of 330 ± 47 mV and −310 ± 44 mV was detected for the positive and negative Al–GO junction, respectively (Figure 3b).

The waveform of the signals shows distinct shape with abrupt jump followed by a slower linear increase, and then plummeting to the baseline upon finger retraction. The baseline of the signal output increased slowly and saturated at around 60 mV after repeated activations due to excessive moisture injection and slow proton diffusion. For the alternating activation between the positive and the negative junctions, the output amplitude and the waveform shape remained stable (Figure 3e). The baseline is pinned around 0 mV in the alternating activation tests due to the counterbalance of the proton diffusion in the opposite directions.

Similar stability tests have also been conducted to the symmetrical Cu–GO, Au–GO, and rGO–GO junction pairs (Figure S10, Supporting Information). Comparable responses of different combinations confirm the stability and the applicability to various conductive coatings. What is more interesting, replacing the metal electrodes by rGO substrates[40] resulted in the same signal level as the Au–GO junctions (Figure S10c,f, Supporting Information), indicating that the universal proton diffusion mechanism works for all kinds of electrodes, no matter chemically reactive with GO or not. Therefore, the structural and chemical compositions can be further simplified by eliminating metal coatings.

For the asymmetrical Au/Al–GO junction pair, when activating the Au–GO junction, lower peak amplitude and large baseline shifts were observed due to sole contribution from the proton diffusion effect (Figure 3c,f). The asymmetrical outputs indicate the independent operation between the two metal–GO junctions on the same GO substrate. When the two junctions are simultaneously activated, the voltage output is the numerical combination of the individual voltage outputs from the two metal–GO junctions (e.g., 0 mV for symmetrical Al–GO junction pair, ±500 mV for asymmetrical Cu/Al–GO junction pair), resulting from the opposite polarities of them.

The robustness of the metal–GO junctions was also demonstrated by applying periodic mechanical deformations during the operations (Video S1, Supporting Information). The minimal background noise at the level of around 1% was measured during repeated bending and shaking indicating excellent strain inertness of the flexible sensor. The material is also inert to "dry" touching (finger in a glove), making an excellent example of bioexclusive tactile sensor. It is worth noting that the temperature variations during touching are identical for the bare and gloved finger, ruling out the possible reason of thermally activated response (e.g., thermoelectricity) (Video S2, Supporting Information).

Another critical parameter for tactile sensing materials is the dynamic responsiveness or the maximum operation frequency, which can be tested by using a linear electrodynamic shaker. The activation frequency is precisely tunable and correlated with the response behavior (**Figure 4**).

Figure 4a–e shows the response waveforms of the Al–GO junctions subjected to actuations at different frequencies at 2, 5, 10, 15, and 20 Hz, respectively. The waveforms are stable and uniform from 2 to 15 Hz with slight baseline upshift due to the relatively long relaxation time of the proton diffusion. When the activation frequency increases to 20 Hz, the waveform starts to become noisy and the baseline is no longer stable due to the vigorous mechanical movement and saturated bioelectrolyte adsorption from the high-frequency repeated microinjections. The sharp peaks on corresponding Fourier transforms are located exactly at the actuating frequency that indicates robust correlation between the actuation and response dynamic (Figure 4f). Higher orders of harmonic oscillation peaks are also prominent (shown for 2, 4, and 10 Hz in the figure), further

Adv. Mater. 2016,
DOI: 10.1002/adma.201506187

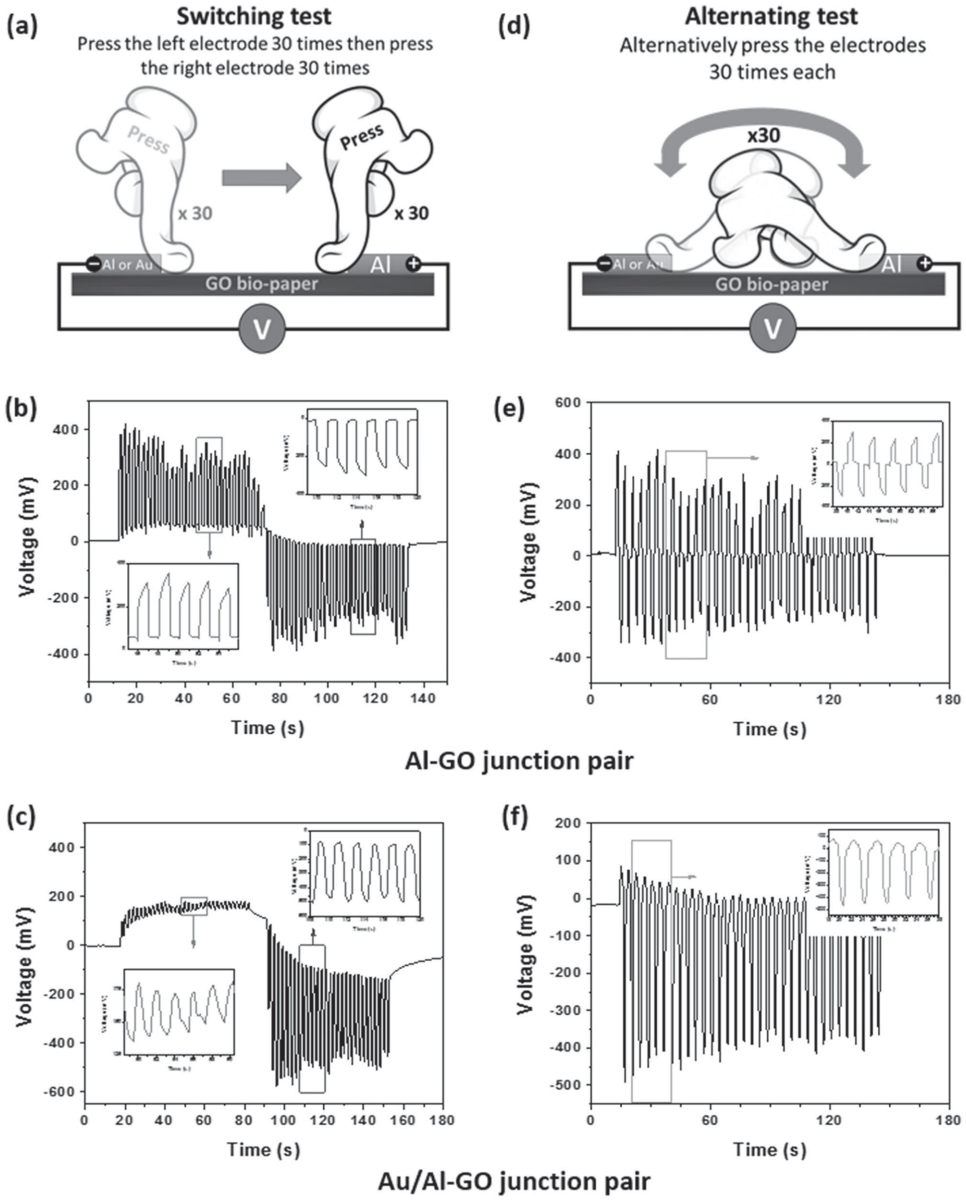

Figure 3. The (a) switching and (d) alternating tests for the stability of the metal–GO junctions as tactile sensing elements (the plus and minus signs on the contacts denotes the polarity of the measuring probes); b,e) open-circuit voltage output of symmetrical Al–GO junction pair and (c,f) asymmetrical Au/Al–GO junction pair under switching and alternating actuations, respectively. The insets show close views of detailed waveform as indicated by frames.

indicating strong coupling of the input events and output signals and stable response across numerous periodic events.

For the highest stable frequency we have tested in this study (15 Hz; Figure 4d), the activation and recovery times (i.e., time needed to rise the signal from 10% to 90% of the full response and vice versa) are very fast, around 21 ms, showing promising potentials for high frequency operation and fast real-time tactile sensing. To the best of our knowledge, this is one of the fastest humidity sensing examples available. Indeed, for instance, an ultrafast GO humidity sensor shows response time in the range of 30–100 ms benefiting from the ultrathin active layer.[47] An optical fiber based humidity sensor shows highly asymmetrical activation and recovery times of 50 ms and more than 700 ms, respectively, due to slower desorption process of the moisture from the active material.[48] Another optical-based fast-response intrinsic humidity sensor has even slower response times of 4.5 and 5.5 s for activation and recovery, respectively.[49] And the response time for the commercially available fast humidity sensors is no less than 100 ms.[47]

To further demonstrate the responsiveness of the tactile sensing metal–GO junctions, to real human finger actuations, the manual touching actuation of the tactile sensor has been tested (Figure S11, Supporting Information). The voltage output reliably records the human finger touching events at different electrodes and at arbitrary frequencies from 0.5 to 5 Hz, demonstrating stable and directly interpretable monitoring of

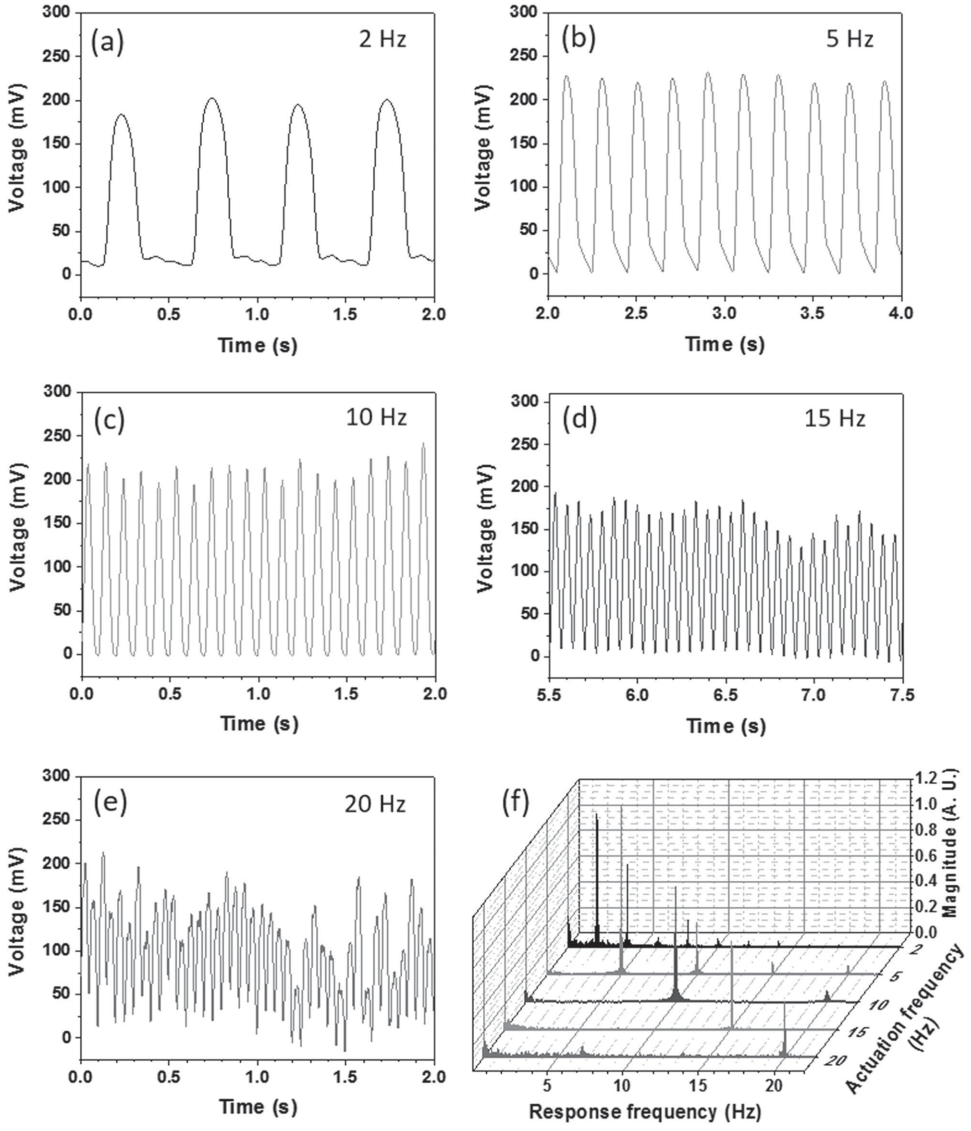

Figure 4. a–e) Frequency variation test on the Al–GO junction, showing stable response to sinusoidal stimuli from 2 to 20 Hz. f) Fast Fourier-transform of the response signal based on the actuation frequency. Higher orders of harmonic response indicate a strong correlation between the input and output.

human-touch events. It is noteworthy that the waveform of the manual touching test is different from that of the linear motor actuations, because the movement of the linear motor is continuous following the sinusoidal pattern while the manual actuation follows the square wave pattern.

It is also noticeable from the previous figures that at low actuation frequencies, the signal baseline upshifts due to the residual water in the metal–GO junction. We have conducted extra low frequency tests at 0.1 and 0.01 Hz to demonstrate the signal stability for quasi-static actuation (Figure S12, Supporting Information). For longer finger press times, the baseline upshifts gradually and the overall signal magnitude increases (Figure 3b; Figure S11, Supporting Information). The baseline stabilizes after the first 3–5 cycles, and the effective signal is constantly higher than 50% of the total magnitude of the electrical output, showing good signal/noise ratio and stability for long-term, low-frequency actuations.

For electronic skins with spatially-resolved tactile sensing, matrices of individual sensing elements should be fabricated and positioned in a grid-like array. In order to explore simple sensing surface regions by utilizing the electrochemical touch sensing, we fabricated a simple version of such a grid with two pairs of orthogonal Al–GO junctions which are capable of addressing nine tactile "pixels" (**Figure 5**; Figure S13, Supporting Information). Specifically, each pair of orthogonally placed electrodes can output three potential levels (i.e., 1, 0, and −1), therefore the two pairs of electrodes act as two ternary digits, which translates to 3×3 distinct states. As we observed, minimal crosstalk happens for the simultaneous operation of these tactile sensors and the small leak signals are due to the slight shift of the touch point from the center of the designated area (Figure S13, Supporting Information).

In this study, we have introduced flexible metal–GO hybrid materials for human-tactile sensing that are exclusively

Adv. Mater. **2016**,
DOI: 10.1002/adma.201506187

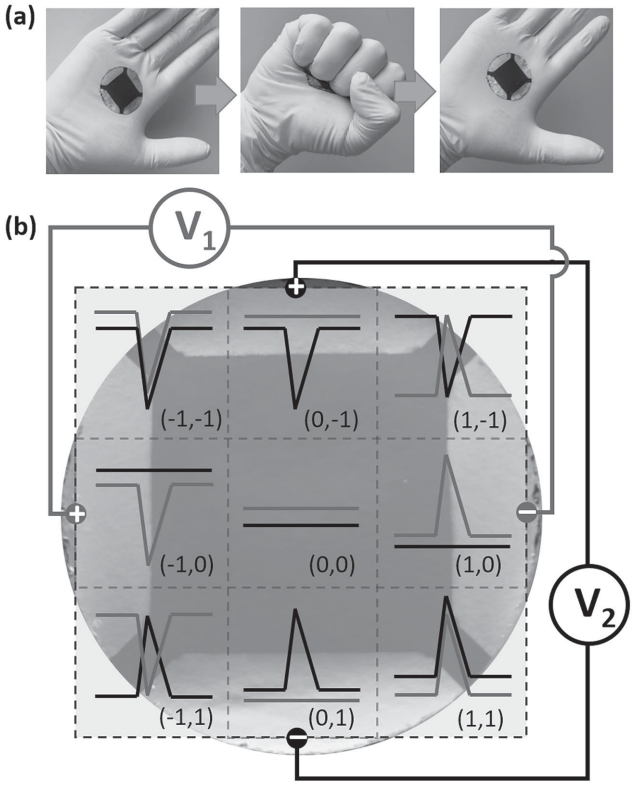

Figure 5. 2D touch-sensing platform (electronic skin) shows the highly independent open-circuit voltage output for the two orthogonally orientated Al–GO junction pairs on the same piece of GO biopaper substrate: a) Excellent bending robustness of the electronic skin withstands repeated fisting in the palm (see Video S3 in the Supporting Information); b) diagram of the 2D sensing circuit and address allocations (the plus and minus signs on the contacts denote the polarity of the measuring probes). The two-digit trinary system is denoted as (V1, V2), and actual waveform of the distinctive response for the nine locations could be found in Figure S13 (Supporting Information).

responsive to real human touch due to the high sensitivity to the microinjection of trace amounts of bioelectrolyte from human fingers with robust electrical potential output. The human-tactile sensitive metal–GO junctions utilize the combination of the unique chemical activity and water permeability of graphene oxide surfaces to generate close to 1 V electric signal per tactile event, which initiates localized electrochemical reaction at metal–GO interfaces. The sensing elements of electronic skins constructed here exhibit spatial-resolved outputs on touching events with programmable signal levels. When compared to the other tactile biosensors, the design introduced in this work is advantageous in facile fabrication, fast response, large continuous signal, and mechanical robustness. The metal–GO junctions show excellent stability of electrical potential response to repeated finger pressing, outstanding signal independency between the individual junctions, and high responsiveness to fast actuations. Because these hybrid metal–GO sensing structures generate electrical potentials when touched, they do not need external power sources in either passive or active modes. Such autonomous devices are excellent candidate for portable applications that require long-term standby and are activated by stored chemical energy generated on-demand.

This ability makes the structures, suggested here, unique among the other known "self-powered" or "zero-power" tactile sensors. For example, a paper-based tactile sensor with the active polypropylene piezoelectric layer sandwiched between silver patterned regular paper substrates can output a maximum signal level of 2 V.[4] However, due to the inherent working principles of piezoelectricity, such tactile sensors only record the transient states of the activation and the signal decoupling between actuation speed and pressure remains a problem. Another passive electronic skin that senses human touch by thermoelectric effect is based on rGO foam.[50] The signal level for normal human touch is around 200 nA and the signal strength is heavily dependent on the temperature gradient across the rGO foam, which is difficult to monitor in real-world applications. Fan et al. have demonstrated a self-powered pressure sensor based on triboelectricity with the maximum signal magnitude reaching 18 V.[51] However, the transient current output caused by the contact electrification mechanism limits its ability to monitor continuous pressure. Other popular designs of sensitive touch sensors such as elastomeric micropillars,[52,53] carbon nanotube elastic composites,[54] or various nanoparticle-filled polymers[55–58] all require electrical energy source for the proper functioning. The power generating metal–GO materials introduced here open a new avenue for both humidity monitoring and biotactile sensing with enhanced power output parameters and sensitivities.

Experimental Section

Materials Fabrication: Graphene oxide biopapers were fabricated following the published procedure.[41] Briefly, 0.76 mL of 0.2 wt% SF aqueous solution was added to 20 mL of 0.15 wt% GO aqueous suspension (pH 11 adjusted by sodium hydroxide) and mixed well. Then 10 mL of the SF–GO mixture was vacuum filtrated against a composite porous membrane (450 nm pore size, Versapor, Pall Life Sciences) and peeled off to get 15 μm thick freestanding GO biopaper.

The metal electrodes (i.e., Al, Cu, and Au) were deposited using electron-beam evaporation (Mark 40, CHA Industries) at 3 Å s^{-1}. The geometries of the electrodes were predetermined by shadow masks and the gap was fixed at 12 mm wide, if not stated otherwise. For the interdigitated finger pattern, the finger width and gap were both 1 mm and the finger length was 14 mm. rGO electrodes were fabricated by reducing the GO layers underneath the aluminum electrode area for 8 h at pH 0.[41] Residual metal after the reduction were rinsed off and checked using XPS to make sure no metal particles were left.

Characterizations: Scanning electron microscopy (SEM, Hitachi SU8230) has been used to image the cross-section of the samples with metal coatings. Energy-dispersive X-ray spectroscopy (EDX, Oxford Instruments) was conducted to draw the elemental map on the cross-sections. To probe the depth profile of the chemical compositions of the GO layers underneath the metal–GO junctions, a scotch tape was used to peel the metal coating and the GO layers, gradually revealing the interfaces of deeper layers. The repeatedly exposed new surfaces of the sample underneath the electrodes were characterized by XPS (Thermo Scientific K-alpha), with the elemental signal from the metal electrodes as the reference for estimated depth. Atomic force microscopy (Dimension-3000, Digital Instruments) was employed to render the surface morphology and the root-mean-square microroughness (within 1×1 μm^2).

The ambient humidity sensing was done in a glove box and the humidity in the chamber was controlled by adjusting the speed and the path length of the dry air passing through a series of water bubblers. The ambient humidity was monitored by a commercial humidity sensor (Model 512, Electro Tech Systems, Inc.) and the device voltage output was

measured by a Fluke 117 digital multimeter. The time-resolved electrical signals were recorded by a potentiostat (VersaSTAT 3, Princeton Applied Research) in open-circuit setup with two electrode connection. All the electrical response tests of the touch sensors were conducted in ambient conditions at 21–23 °C and 35–45 RH%. The frequency tests were realized by a combination of an electrodynamic shaker (LW126.151-9, Labworks Inc.) and a sinusoidal wave function generator (SC-121 Sine Servo Controller system, Labworks Inc.), scanning from 2 to 20 Hz.

Supporting Information

Supporting Information is available from the Wiley Online Library or from the author.

Acknowledgements

The authors thank the financial support from the Air Force Office for Scientific Research FA9550-14-1-0269 Award (K. Hu and R. Ma), National Science Foundation CBET Award No. 1401720 (S. Zhang), National Natural Science Foundation of China Grant 51473100 (R. Xiong) and Grant 51572040 (H. Guo), and China Scholarship Council (R. Xiong and H. Guo).

Received: December 13, 2015
Revised: January 16, 2016
Published online:

[1] M. I. Tiwana, S. J. Redmond, N. H. Lovell, *Sens. Actuators A Phys.* **2012**, *179*, 17.
[2] P. Dario, C. E. Piaggio, *Sensors and Sensory Systems for Advanced Robots*, Springer, Berlin **2012**.
[3] R. S. Dahiya, M. Valle, *Robotic Tactile Sensing: Technologies and System*, Springer, Netherlands **2012**.
[4] Q. Zhong, J. Zhong, X. Cheng, X. Yao, B. Wang, W. Li, N. Wu, K. Liu, B. Hu, J. Zhou, *Adv. Mater.* **2015**, *27*, 7130.
[5] W. Wu, X. Wen, Z. L. Wang, *Science* **2013**, *340*, 952.
[6] Z. L. Wang, *Adv. Mater.* **2007**, *19*, 889.
[7] C. Pan, L. Dong, G. Zhu, S. Niu, R. Yu, Q. Yang, Y. Liu, Z. L. Wang, *Nat. Photonics* **2013**, *7*, 752.
[8] C. Pang, G.-Y. Lee, T.-i. Kim, S. M. Kim, H. N. Kim, S.-H. Ahn, K.-Y. Suh, *Nat. Mater.* **2012**, *11*, 795.
[9] H.-B. Yao, J. Ge, C.-F. Wang, X. Wang, W. Hu, Z.-J. Zheng, Y. Ni, S.-H. Yu, *Adv. Mater.* **2013**, *25*, 6692.
[10] B. C. K. Tee, C. Wang, R. Allen, Z. Bao, *Nat. Nanotechnol.* **2012**, *7*, 825.
[11] S. C. B. Mannsfeld, B. C. K. Tee, R. M. Stoltenberg, C. V. H. H. Chen, S. Barman, B. V. O. Muir, A. N. Sokolov, C. Reese, Z. Bao, *Nat. Mater.* **2010**, *9*, 859.
[12] H. Vandeparre, D. Watson, S. P. Lacour, *Appl. Phys. Lett.* **2013**, *103*, 204103.
[13] S. Singamaneni, M. E. McConney, M. C. LeMieux, H. Jiang, J. O. Enlow, T. J. Bunning, R. R. Naik, V. V. Tsukruk, *Adv. Mater.* **2007**, *19*, 4248.
[14] S. Singamaneni, M. C. LeMieux, H. P. Lang, C. Gerber, Y. Lam, S. Zauscher, P. G. Datskos, N. V. Lavrik, H. Jiang, R. R. Naik, T. J. Bunning, V. V. Tsukruk, *Adv. Mater.* **2008**, *20*, 653.
[15] Y. Yang, H. Zhang, Z.-H. Lin, Y. S. Zhou, Q. Jing, Y. Su, J. Yang, J. Chen, C. Hu, Z. L. Wang, *ACS Nano* **2013**, *7*, 9213.
[16] G. Zhu, W. Q. Yang, T. Zhang, Q. Jing, J. Chen, Y. S. Zhou, P. Bai, Z. L. Wang, *Nano Lett.* **2014**, *14*, 3208.
[17] F. Yi, L. Lin, S. Niu, J. Yang, W. Wu, S. Wang, Q. Liao, Y. Zhang, Z. L. Wang, *Adv. Funct. Mater.* **2014**, *24*, 7488.
[18] Y. Zang, F. Zhang, C.-a. Di, D. Zhu, *Mater. Horiz.* **2015**, *2*, 140.
[19] C.-Y. Lee, G.-B. Lee, *Sens. Lett.* **2005**, *3*, 1.
[20] Z. L. Wang, J. Song, *Science* **2006**, *312*, 242.
[21] S. Xu, Y. Qin, C. Xu, Y. Wei, R. Yang, Z. L. Wang, *Nat. Nanotechnol.* **2010**, *5*, 366.
[22] F.-R. Fan, Z.-Q. Tian, Z. L. Wang, *Nano Energy* **2012**, *1*, 328.
[23] R. H. Mole, *J. Physiol.* **1948**, *107*, 399.
[24] C. Jiang, S. Markutsya, Y. Pikus, V. V. Tsukruk, *Nat. Mater.* **2004**, *3*, 721.
[25] Z. Chen, C. Lu, *Sens. Lett.* **2005**, *3*, 274.
[26] H. Farahani, R. Wagiran, M. Hamidon, *Sensors* **2014**, *14*, 7881.
[27] M. C. LeMieux, M. E. McConney, Y.-H. Lin, S. Singamaneni, H. Jiang, T. J. Bunning, V. V. Tsukruk, *Nano Lett.* **2006**, *6*, 730.
[28] P. Mukhopadhyay, R. K. Gupta, *Graphite, Graphene, and their Polymer Nanocomposites*, CRC Press, Boca Raton, **2012**.
[29] D. R. Dreyer, S. Park, C. W. Bielawski, R. S. Ruoff, *Chem. Soc. Rev.* **2010**, *39*, 228.
[30] V. Singh, D. Joung, L. Zhai, S. Das, S. I. Khondaker, S. Seal, *Prog. Mater. Sci.* **2011**, *56*, 1178.
[31] J. Zhao, G.-Y. Zhang, D.-X. Shi, *Chin. Phys. B* **2013**, *22*, 057701.
[32] Y. Sun, G. Shi, *J. Polym. Sci., Part B: Polym. Phys.* **2013**, *51*, 231.
[33] L. Dai, *Acc. Chem. Res.* **2012**, *46*, 31.
[34] M. F. El-Kady, V. Strong, S. Dubin, R. B. Kaner, *Science* **2012**, *335*, 1326.
[35] K. Hu, D. D. Kulkarni, I. Choi, V. V. Tsukruk, *Prog. Polym. Sci.* **2014**, *39*, 1934.
[36] E. L. Wolf, *Applications of Graphene: An Overview*, Springer, New York, **2014**.
[37] K. Hu, M. K. Gupta, D. D. Kulkarni, V. V. Tsukruk, *Adv. Mater.* **2013**, *25*, 2301.
[38] Y. Yin, K. Hu, A. M. Grant, Y. Zhang, V. V. Tsukruk, *Langmuir* **2015**, *31*, 10859.
[39] R. Xiong, K. Hu, A. M. Grant, R. Ma, W. Xu, C. Lu, X. Zhang, V. V. Tsukruk, *Adv. Mater.* **2015**, DOI: 10.1002/adma.201504438
[40] K. Hu, L. S. Tolentino, D. D. Kulkarni, C. Ye, S. Kumar, V. V. Tsukruk, *Angew. Chem. Int. Ed.* **2013**, *52*, 13784.
[41] K. Hu, V. V. Tsukruk, *Chem. Mater.* **2015**, *27*, 6717.
[42] B. Schittek, R. Hipfel, B. Sauer, J. Bauer, H. Kalbacher, S. Stevanovic, M. Schirle, K. Schroeder, N. Blin, F. Meier, G. Rassner, C. Garbe, *Nat. Immunol.* **2001**, *2*, 1133.
[43] X. Cao, D. Qi, S. Yin, J. Bu, F. Li, C. F. Goh, S. Zhang, X. Chen, *Adv. Mater.* **2013**, *25*, 2957.
[44] F. Zhao, H. Cheng, Z. Zhang, L. Jiang, L. Qu, *Adv. Mater.* **2015**, *27*, 4351.
[45] S. Pei, H.-M. Cheng, *Carbon* **2012**, *50*, 3210.
[46] Y. Li, K. Fan, H. Ban, M. Yang, *Sens. Actuators, B* **2016**, *222*, 151.
[47] S. Borini, R. White, D. Wei, M. Astley, S. Haque, E. Spigone, N. Harris, J. Kivioja, T. Ryhänen, *ACS Nano* **2013**, *7*, 11166.
[48] J. Mathew, Y. Semenova, G. Farrell, *Sens. Actuators, A* **2012**, *174*, 47.
[49] G. Rajan, Y. M. Noor, B. Liu, E. Ambikairaja, D. J. Webb, G.-D. Peng, *Sens. Actuators, A* **2013**, *203*, 107.
[50] C. Hou, H. Wang, Q. Zhang, Y. Li, M. Zhu, *Adv. Mater.* **2014**, *26*, 5018.
[51] F.-R. Fan, L. Lin, G. Zhu, W. Wu, R. Zhang, Z. L. Wang, *Nano Lett.* **2012**, *12*, 3109.
[52] H. Park, Y. R. Jeong, J. Yun, S. Y. Hong, S. Jin, S.-J. Lee, G. Zi, J. S. Ha, *ACS Nano* **2015**, *9*, 9974.
[53] A. Alfadhel, J. Kosel, *Adv. Mater.* **2015**, *27*, 7888.
[54] J. Park, Y. Lee, J. Hong, Y. Lee, M. Ha, Y. Jung, H. Lim, S. Y. Kim, H. Ko, *ACS Nano* **2014**, *8*, 12020.
[55] M. Segev-Bar, H. Haick, *ACS Nano* **2013**, *7*, 8366.
[56] N. Olichwer, E. W. Leib, A. H. Halfar, A. Petrov, T. Vossmeyer, *ACS Appl. Mater. Interfaces* **2012**, *4*, 6151.
[57] T. Vossmeyer, C. Stolte, M. Ijeh, A. Kornowski, H. Weller, *Adv. Funct. Mater.* **2008**, *18*, 1611.
[58] F. Zhao, Y. Zhao, H. Cheng, L. Qu, *Angew. Chem. Int. Ed.* **2015**, *54*, 14951.